Expansion modelling based on cracking induced by the formation of new phases in concrete

Stéphane Multon, Alain Sellier

Expansion modelling based on cracking induced by the formation of new phases in concrete

Stéphane Multon [a*] and Alain Sellier [a]

[(a)] *Université de Toulouse; UPS, INSA; LMDC (Laboratoire Matériaux et Durabilité des Constructions); 135, avenue de Rangueil; F-31 077 Toulouse Cedex 04, France*

Abstract

Unexpected expansion can be a cause of damage in quasi-brittle materials such as concrete, fired clays or rocks. Such expansions can be due to chemical reactions (alkali-silica reaction – ASR, sulfate attack) or physical phenomena (frost, transport of fluids). Expansion is caused by two main mechanisms: matrix deformation due to the pressure initiated by the formation of new phases in the porosity of the material, and matrix cracking, which increases the apparent swelling of the matrix. In this work, a poromechanical model is proposed to reproduce expansion in materials resulting from single or multiple pressures. In this model, plastic deformation is used to represent permanent strain due to diffuse cracking induced by the pressure. In the case of expansion in quasi-brittle materials, the permanent deformations induced by the pressure are anisotropic to take account of the impact of the initial material anisotropy and stress anisotropy on cracking. The model is then coupled with a damage model and used to evaluate the opening of localized cracks due to a pressure gradient in a laboratory specimen.

Keywords

Anisotropy, cracking, expansion, plasticity, pressure.

[*] Corresponding author, *e-mail address:* multon@insa-toulouse.fr (Stéphane Multon)

1. Introduction

Damage due to expansion in materials decreases the service life of structures. Unexpected expansion can be responsible for cracking in concrete, fired clays or other quasi-brittle materials and mechanical modelling should be able to evaluate their behaviour at material and structure scales. External or internal chemical attacks (Alkali-Silica Reaction – ASR [1], Delayed Ettringite Formation – DEF [2], external sulfate attack [3], expansion of resins embedded in quasi-brittle materials [4]) or physical phenomena (frost [5]) can be the cause of such swelling and lead to a decrease in the strength of the materials affected. For quasi-brittle materials, irreversible deformation due to cracking induced by pressure is the main cause of the positive strain of expansion. The balance between local stresses around expansive new phases and stresses due to external loading leads to anisotropic cracking. Given the dependence of the pressure on environmental conditions, the development of such expansions can also lead to deformation gradients both in real structures and in specimens studied under laboratory conditions. The consequence is the opening of localized cracks on the skin of the concrete.

Modelling should be able to distinguish and to assess the contribution of each mechanism: pressure, diffuse cracking due to material damage, and localized cracking due to pressure gradient.

In this work, a poromechanical model is proposed and used to quantify expansion in concrete. First, the determination of the pressure according to the volume increase of new phases in the material is described within the framework of poromechanics [6], [7]. In particular, the case of alkali-silica reaction, for which pressure occurs in inclusions (aggregate) embedded in the material (concrete) is addressed as a case for which up-scaling and multiple pressures should be considered. Plasticity is commonly used to represent permanent strain of quasi-brittle materials [8], [9]. In the present work, plastic deformation is adopted to model the permanent strain due to the diffuse cracking caused by the pressure. The criteria associated with these deformations are orthotropic so as to

consider the impact of an anisotropic stress state on expansions [10], [11]. The model is then used to reproduce the swelling anisotropy induced either by the anisotropic initial strength of certain materials, or by the anisotropy due to the stress state. The analysis highlights the importance of cracking in the mechanisms of expansion in concrete.

2. Pressure

Because of their low strength in tension, the elastic deformation of quasi-brittle materials under internal pressure is small. Cracking thus plays an important role in deformations and has to be accurately determined. After cracking, the evolution of irreversible deformation under the effect of expansive phases is still driven by their pressures. Therefore, the same care has to be taken when evaluating pressure or anisotropic permanent strains corresponding to the induced cracking.

2.1 Pressure due to the formation of new phases

The pressure induced by the formation of new phases in materials depends on the amount and the nature of the reactive components [12]–[21], on the structure of the material porosity [22]–[25] and on the capability of the porous material to tolerate induced tension. The interactions between the swelling inclusions and the matrix determine the pressure developed in the swelling phase. In this work, the pressure, p_i, in the porous material due to inclusion *i* is determined in the framework of poromechanics [6], [7] through the following equation:

$$p_i = M_i \cdot \left(\varphi_i - \varphi_i^0 - \varphi_p \ - \varphi_{cr}\right) \qquad (1)$$

with:

M_i the Biot Modulus related to the inclusions,

φ_i, the volumetric fraction of porosity filled by the inclusions related to the skeleton deformation [23]. It can be assessed from the growth of the new phases in relation to crystallization pressure [12], [13], [23] or to the volume produced by chemical reaction [14], [26].

φ_i^0 is the volumetric fraction of new phases leading to little expansion during the reaction for mechanical reasons (migration in porosity [25], [27]–[29], formation in pores too

large to induce pressure [14], [22], [30]) or chemical reasons (composition of the phases [31]–[33] or non-expansive surface absorption [34]). It is taken to be proportional to the pressure:

$$\varphi_i^0 = \varphi_{ref} \cdot \frac{p_i}{p_{ref}} \quad (2)$$

φ_{ref} is a reference volume. It corresponds to the volume of new phases formed for the pressure p_{ref} that leads to the first cracking at material scale in free swelling conditions. It can be related to the pore distribution [14], [27] or be calibrated to obtain the delay at the beginning of the expansion curve.

φ_p is the volumetric deformation – due to elasticity – of porosity filled by the inclusion of new phases, and delayed deformation (diffuse cracking due to the pressure and structural cracks are not considered in this term but in φ_{cr} as explained below), which can be calculated with b_i, the Biot coefficient related to the expansive inclusions:

$$\varphi_p = b_i \cdot (\varepsilon - \varepsilon_{cr} - \varepsilon_{an}) \quad (3)$$

Here, ε is the mechanical deformation of the porous material, and ε_{cr} its deformation due to cracking induced by the pressure. The impact of ε_{cr} on pressure is considered in (1) with an interaction coefficient of 1, and thus greater than the Biot coefficient used in (3). ε_{an} is the deformation due to structural cracks that are not connected to the sites of formation of inclusions and so cannot have a direct impact on the pressure.

In equation (1), φ_{cr} is the volume of diffuse cracks caused by the pressure; it is equal to the volumetric deformation of the porous material due to the diffuse cracking ε_{cr}. In this equation, for the sake of simplicity, this volume is assumed to be totally filled by the new phases. The main assumption of the model is then that the new phases can migrate only toward the cracks they have themselves created.

The role of φ_{cr} in Equation (1) is particularly important for the modelling of such phenomena. If at least one direction is free of compressive stress in the material, the pressure p_i cannot increase very greatly as cracking is possible perpendicularly to the free direction. This is taken into account through φ_{cr}. If φ_{cr} increases, the stabilization of the pressure p_i can be obtained. This stabilization of the pressure is necessary to obtain

realistic stress in cases of restraint, as observed in experimentally [30], [35]–[38]. This point is highlighted in the part that focuses on cracking.

M_i, the Biot Modulus related to the inclusions, depends on the volume of new phases φ_i and on the mechanical properties of the matrix (bulk modulus K_m) and the inclusions [6], [7], [24]. m is the subscript related to the matrix, including solid and porosity that is not filled by the new phase inclusions. It is evaluated with the following equation:

$$\frac{1}{M_i} = \frac{b_i - \varphi_i}{K_m} + \frac{\varphi_i}{K_i} \quad (4)$$

If the new phases are taken to be spherical and embedded in a homogeneously solid matrix [24]; b_i, the Biot coefficient related to the inclusion, can be estimated using a Mori-Tanaka scheme for the estimation of the bulk modulus, K, of the porous material [39]:

$$b_i = 1 - \frac{K}{K_m} = \frac{\varphi_i(3K_m + 4\mu_m)}{(3K_m\varphi_i + 4\mu_m)} \quad (5)$$

with μ_m, the shear modulus of the matrix.

For simplicity, the Biot coefficient is evaluated in a linear context here, from the mechanical properties and volumes of inclusions (Equation (5)) without consideration of the shape of the porosity filled by the new phases. More precise quantification could be obtained by taking account of the shape of filled cracks as proposed in [26], [27], [40]. In the present work, the non-linearity due to the combination with diffuse cracking caused by pressure, creep [41] and structural damage [42] is considered differently, by resorting to damage theory [53].

The advancement of the new phases production can be evaluated with physicochemical considerations or empirical laws. The aim of the paper is to focus on mechanical considerations. As the chemical advancement is usually not impacted by mechanical conditions in the case of the expansion due to new phases formation in concrete [43], the chemical advancement can be separated of the mechanical problem. The equations presented in this paper can thus be used whatever the approach applied to determine the chemical advancement (theoretical or empirical approaches [12], [15], [17], [18], [20], [21], [25], [44]).

The volumetric fraction of porosity filled by the inclusions can be considered as a data and its determination is summed up by the following equation:

$$\varphi_i(t) = n_i^{max} \cdot \varphi_i^{mol} \cdot A(t) \quad (6)$$

With n_i^{max}, the maximal number of moles of the new products which can be formed in the material, φ_i^{mol}, the molar volume of the new phases and $A(t)$, the advancement of the reaction.

2.2 Case of porous materials embedded in another material

In some cases, the expansive inclusions can be formed in porous materials embedded in other materials. For example, Alkali-Silica Reaction (ASR) expansion can occur in aggregates embedded in concrete [45]–[48]. In this situation, scale-up is necessary to evaluate, firstly, the impact of the formation of new phases on the lower scale matrix (LS in Figure 1, for example the aggregate) and, secondly, the impact of the pressure of the lower scale matrix on the macro scale (MS in Figure 1, for example, the concrete). The volumetric fraction of the embedded material per volume of the macro scale material is referenced as φ_a . Moreover, the material embedded in the macro scale material can have different sizes and volumetric fractions and lead to multiple pressures [4], [27]. The pressure of each fraction p_a is different and should be evaluated separately.

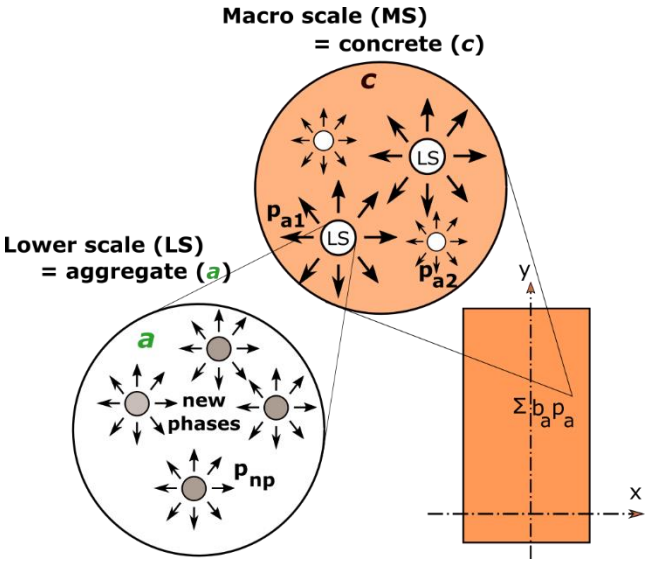

Figure 1: Porous material (Lower Scale, LS) embedded in another porous material (Macro Scale, MS)

The three equations of the multi-scale approach used to evaluate the pressure due to the new phases p_{np} on the lower scale matrix (Equation (7)), the resulting pressure of the lower scale p_a on the macro scale (Equation (8)) and finally the action of the multiple pressures p_a of the lower scale matrix on the macro scale (Equation (9)) are:

$$\begin{cases} p_{np} = M_{np} \cdot \left(\varphi_{np} - \varphi_{np}^{0} - \varphi_p - \frac{\varphi_{cr}}{\varphi_a}\right) \downarrow From\ new\ phases\ to\ lower\ scale \\ p_a = b_{np} \cdot p_{np} \qquad \downarrow From\ lower\ scale\ to\ macro\ scale \\ \tilde{\sigma}_s = K_m \cdot \left(\varepsilon - \varepsilon_{an}\right) - \sum_a b_a \cdot p_a \end{cases} \quad (7) \quad (8) \quad (9)$$

The interactions between the three equations and the different terms of the equations are explained in the three following subparts:

Pressure of new phases (NP) on the lower scale (LS) material

At the lower scale, the inclusion *i* (*i = np* at this scale) is the new phases, and the matrix, m (*m = a* at this scale) is the lower scale (LS) matrix. As the expansive inclusions are formed at the lower scale (Figure 1), the pressure induced by the formation of new phases on the LS matrix can be defined from Equation (7).

φ_{np}, φ_{np}^{0} and φ_p are defined above and have to be determined per unit of volume of the lower scale matrix (here the aggregate). M_{np} and b_{np} related to the new phases are evaluated from Equations (4) and (5).

As the cracks induced by the pressure of the new phases are usually connected with the cracks at macro scale [48], the volume of cracks φ_{cr} in which the new phases can migrate is taken to be the crack volume available in the macro scale material. At the scale of the aggregate, this volume has to be normalized according to the volumetric fraction of aggregate φ_a in order to be obtained per unit of volume. Consequently, the impact of the crack volume on pressure is fully considered at this lower scale.

Pressure of the lower scale (LS) material on the macro scale (MS) material

At the macro scale (Figure 1), the inclusion *i* (*i = a* at this scale) is the aggregate, and the matrix m (*m = c* at this scale) is the concrete. M_a and b_a, related to the aggregate, are evaluated from Equations (4) and (5).

The material at macro scale subjected to the pressure of the aggregate is under tension. Because of its low tensile strength, the impact of its rigidity on aggregate pressure is negligible compared to the impact of the crack volume, which was considered at the lower scale. The pressure induced by the lower scale (aggregate) on the macro scale (concrete) can thus be evaluated from Equation (8).

Consequence on pressure at the macro scale (MS) in case of expansive inclusions having different sizes

As proposed in [7], [24], [26], the impact of multiple pressures on the macro scale material can be obtained by summing the pressure, taking Biot coefficients into account. The constitutive equation for the mean stress $\tilde{\sigma}_s$ at macroscopic scale is then Equation (9).

In this case of multiple pressures, the volume of cracks of the macro scale material (φ_{cr} in equation (7)) has to be distributed among the different fractions of aggregates (φ_a). In this work, the distribution is assumed to be proportional to the volume of the new phases φ_{np_a} leading to cracking (so the volume of phases higher than φ_{np}^0 in equation (10)). For material containing several sizes, *a*, of aggregate, it is necessary to distinguish the new phases created by each aggregate: φ_{np_a} is the volumetric fraction of new phases created in aggregate *a* and $\varphi_{np\_a}^0$ is the volumetric fraction of new phases necessary to start cracking in aggregate *a*. Thus, the volume of the crack induced by aggregate *a* is evaluated by (10):

$$\varphi_{cr}^a = \frac{\langle \varphi_{np\_a} - \varphi_{np\_a}^0 \rangle^+}{\sum_a \langle \varphi_{np\_a} - \varphi_{np\_a}^0 \rangle^+} \varphi_{cr} \tag{10}$$

For expansion in quasi-brittle materials, the model considers damage through a coupling with the modelling presented in [42]: the coupling method consists of affecting $\tilde{\sigma}_s$ by the damage according to the principle already presented in [11] (Equation (11)):

$$\sigma_s = \tilde{\sigma}_s \ (1 - D) \tag{11}$$

The damage variable, D, depends on the permanent strain related to the diffuse cracking and on the effective stress $\tilde{\sigma}_s$ due to the external loading.

Creep of the matrix, simultaneous with expansion, is also considered so as to obtain a realistic evaluation of concrete damage at micro and macro scales [11], [49]: ε_{an} is the inelastic strain due to creep and cracking at the macro-scale. Creep is considered through the model presented in [41] combined with the damage model proposed in [42] according to the combination method described in [11].

3. Cracking

3.1 Diffuse cracking due to pressure

In stress free conditions, the diffuse cracking induced by the pressure can be isotropic (sulfate attack [38]) or anisotropic (alkali-silica reaction [50], [51], and frost in fired clays [52]). In the absence of external loading, anisotropic expansion can be explained by the initial anisotropy of the materials, for instance by the shape and the orientation of the expansive inclusion (Figure 2). At the scale of the porous material, the mean stress field is homogeneous. For uniformly distributed spherical inclusions, no direction is preferential in stress free conditions (Figure 2). In this case, the cracking direction should be isotropic at the representative volume scale. For flattened inclusions oriented in a preferential direction, the stress induced by the pressure at the points with the smallest radius is larger than anywhere else (Figure 2). This leads to anisotropic cracking. The presence of water pockets under the expansive inclusions can also cause orientation of cracking [53]. In the absence of loading, this effect can be evaluated through the following anisotropic cracking criteria f_i according to f_t, the tensile strength of the porous material:

$$\begin{cases} f_I = k_I \cdot p_{np} - f_t \\ f_{II} = k_{II} \cdot p_{np} - f_t \\ f_{III} = k_{III} \cdot p_{np} - f_t \end{cases} \quad (12)$$

k_i are the stress concentration factors in the three main directions of the aggregate shape and p_{np} the pressure of the new phases produced in the embedded materials and responsible for the diffuse cracking.

If one of these criteria f_i becomes higher than zero, cracks appear along this direction. In the absence of loading, the cracks appear first in the plane perpendicular to the direction having the largest stress concentration factor.

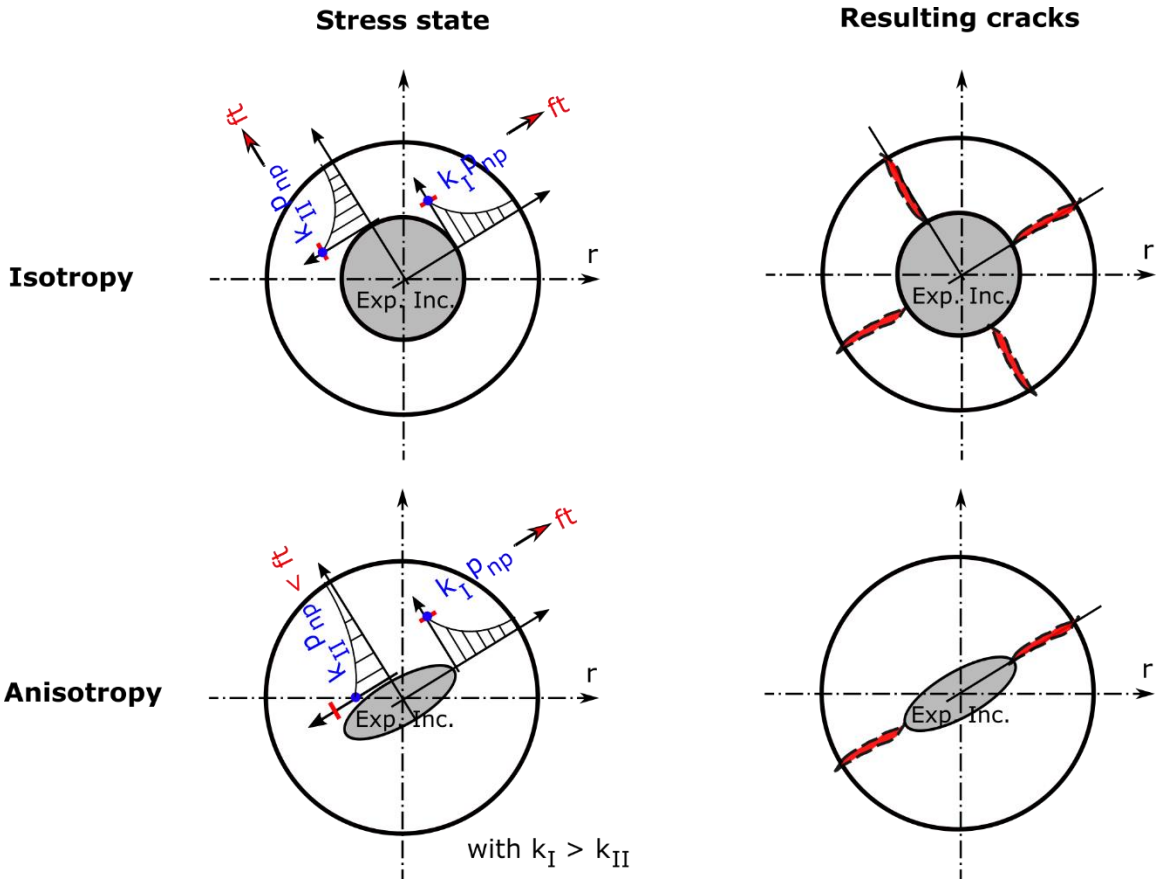

Figure 2: Ortho-radial stress state around spherical and penny-shaped inclusions from continuous mechanics and resulting cracks

With the simplified assumption of spherical inclusions, k_I is independent of the orientation and can be evaluated in a linear context from the proportion of new phases:

$$k_I = k_{II} = k_{III} = \frac{1 + 2 \cdot \varphi_{np\_a}}{2 \cdot \left(1 - \varphi_{np\_a}\right)} \tag{13}$$

If the material is damaged by multiple pressures, the single stress used in the plastic criterion at the macro-scale has to consider all the crack initiation possibilities at smaller scales. For this purpose, the local stress is evaluated in proportion to the pressures

weighted by the volume of new phases φ_{np_a} leading to cracking (so the volume of phases higher than φ_{np}^{0}).

According to the geometry of the inclusion, the stress concentration factor can be dependent on the direction (Figure 2). For orthotropic inclusions, the ratio between the stress concentration factors in the three main directions (I, II, III) of a penny shaped inclusion *a* (Figure 2) is defined by equation (14):

$$k_{II} = k_{III} = \rho_{ani} \cdot k_I \quad (14)$$

ρ_{ani} is the rate of anisotropy (less than 1).

If ρ_{ani} is equal to 1, the cracking in stress-free conditions remains isotropic in the absence of external loading. If ρ_{ani} is less than 1, the cracking in stress-free conditions becomes orthotropic and occurs first in the plane perpendicular to the direction *I* (Equation (14), Figure 2). This leads to anisotropic expansions.

3.2 Anisotropy of cracking due to macroscopic stress state

Under anisotropic mechanical loading, expansions are anisotropic [36], [37], [43], [54]–[57]. For different natures of new phases (alkali silica gels or ettringite), a difference of 1 MPa in stress compared to the mean stress in the material is sufficient to cause anisotropic expansion [36], [38], [54], [58].

Expansion anisotropy in materials subjected to loading is due to anisotropy of cracking. It can be explained by the balance between the stresses induced by expansion around the inclusion and the stresses due to external conditions. In stress free conditions, the material is subjected to tensile stress around the expansive inclusions and the resulting crack distribution is theoretically isotropic if the inclusions are isotropic and uniformly distributed (Figure 3). Under compressive stresses, the tensile stresses are reduced (or even cancelled by the compressive stresses due to the external loading) in the direction parallel to the compressive stress and cracking is prevented in the direction perpendicular to the applied load (Figure 3). The stress state is not modified along the direction perpendicular to loading and cracking appears when, locally, the stress reaches the tensile strength (Figure 3). This explains why the cracks are usually parallel to the compressed direction or to the restraint whatever the nature of the new phases [30], [35], [38], [43].

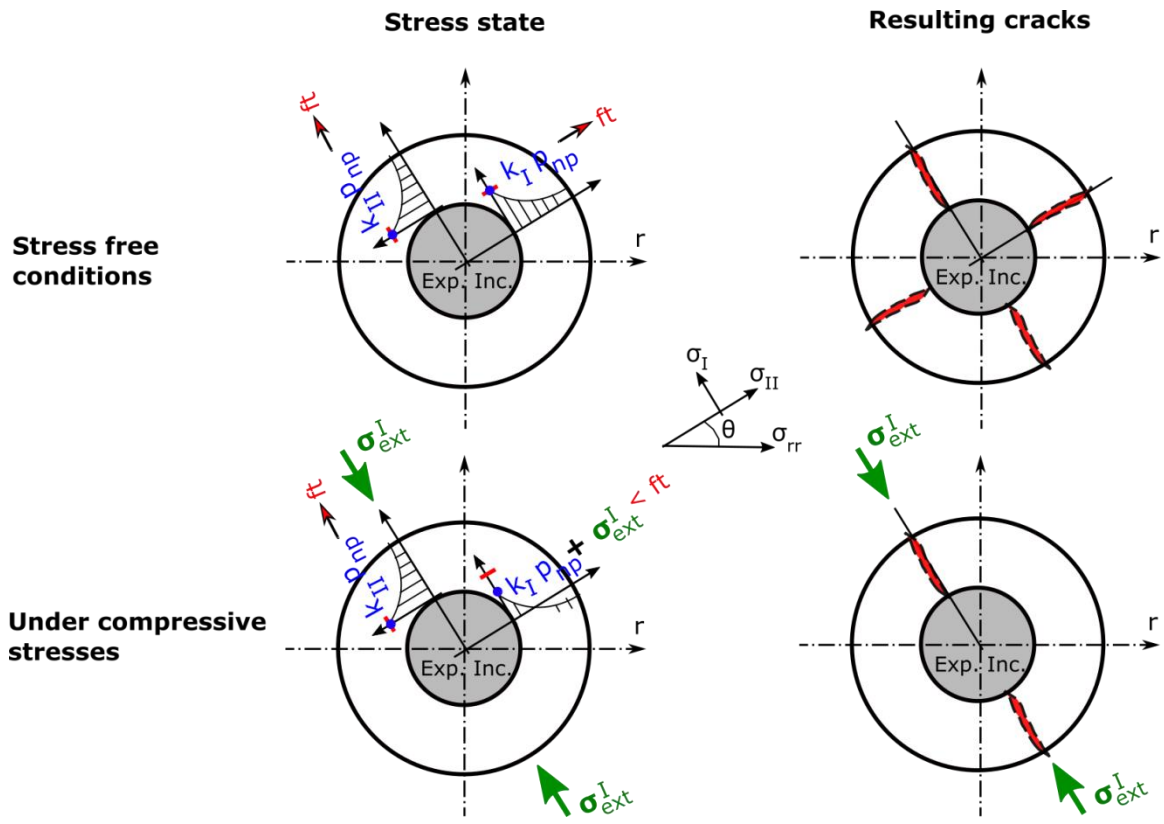

Figure 3: Idealized stress state around expansive inclusion, and resulting cracks. Due to the stress field shift towards compression, the failure criterion cannot be reached perpendicular to the applied compression, but only parallel to it

Once cracks occur in one direction, the following expansions change since the new phases can flow into or be formed in the cracks and pressure can be preferentially exerted perpendicular to the cracks. In cases of compression along two directions, cracking can occur parallel to the loading plane. In presence of loading, the anisotropic diffuse cracking can be evaluated through the following criteria f_i:

$$\begin{cases} f_I = k_I \cdot p_{np} + \tilde{\sigma}_I - f_t \\ f_{II} = k_{II} \cdot p_{np} + \tilde{\sigma}_{II} - f_t \\ f_{III} = k_{III} \cdot p_{np} + \tilde{\sigma}_{III} - f_t \end{cases} \quad (15)$$

with $\tilde{\sigma}_I$ the external stress in the material without damage (effective stress) in the main direction I of stresses (in this case, the stress concentration factors k_I are computed in the main direction of stresses).

For cracking to occur in stress-free conditions, the local tensile stress, equal to $k_I \cdot p_{np}$, has to be greater than the local strength f_t (Equation (12)). In cases of compressive stress induced by external loading, $\tilde{\sigma}_I$ is negative (Equation (15)). To lead to cracking, the local stress induced by the pressure ($k_I \cdot p_{np}$) has to be higher than the sum of the tensile strength and the absolute value of the compressive stress.

As the loading stress $\tilde{\sigma}_I$ is limited by the tensile strength f_t in the direction I [42], the diffuse cracking depends directly on the pressure of the new phases for a material cracked by external loading. The criterion becomes:

$$f_I = k_I \cdot p_{np} \tag{16}$$

If the external principal stresses do not coincide with the material main directions, the stress concentration factors are determined in the principal directions of stresses according to elliptic approximations. Thus, the cracks orientation is mainly driven by the external principal stresses which is usually observed in real cases.

3.3 Pressure evolution during diffuse cracking

The volume of new phases changes over time: frost can disappear with increasing temperature, alkali-silica gels can lose water when exposed to dry conditions, etc. After such modifications, a large part of the expansion remains unchanged [5], [50], [59], so the diffuse cracking induced by expansive phenomena does not appear to be reclosed. This can be explained by the relative displacements of the lips of rough cracks. Lip displacements lead to irreversible strains. This situation is modelled by means of the plasticity theory that has already been used to represent permanent strain in quasi-brittle materials [8], [9]. A plastic criterion is thus used to manage the permanent strain due to the diffuse cracking induced by the pressure. It has already been used to model ettringite formation [60] and alkali-silica reaction [61] expansions subjected to stress at macro-scale. In these previous works, the anisotropy of cracking with loading (Figure 3) was already considered but, in the present paper, the plastic criterion is modified to also consider a possible initial anisotropy of the material through the inclusion shape.

The behaviour of quasi-brittle materials subjected to expansion after first cracking has to be linked to experimental observations performed on specimens under restraint or applied stresses:

- Under restraint, the expansive mechanism leads to compressive stresses at macroscopic scale [30], [35]–[38]. In three experimental studies [30], [35], [36], rigid steel frames were used to strongly restrained expansion in one direction (the rigidity of the frames were largely upper than the rigidity of concrete specimens). In these three cases, for concrete expansion due to ASR or ettringite formation, the free swelling ranges from 0.1% to 8% and the resulting macroscopic uniaxial stress due to restraint lies between only 1 and 8 MPa [30], [35], [36] (Figure 4). The relation between free swelling and restraining stress appears to be quite linear between 0 and about 0.4%, with an increase of 1 MPa per 0.1% of free expansion. After 4 MPa, the increase of uniaxial stress with the free expansion slows down. In comparison, for a material with a Young's modulus of 30,000 MPa, an expansion of only 0.1% imposed on a perfectly elastic material would lead to restraint stress of 30 MPa.
- Under applied loading, the application of uniaxial compressive stresses of about 5 MPa is usually sufficient to stop expansion of about 0.2% in the loaded direction [43], [55]. Beyond this stress, the creep strains in the loaded direction appear to be the same as for creep in the material without expansion [43], [54], [55].

In these experiments, restraint and applied loading were uniaxial, and cracks could propagate in plans perpendicular to free directions. The new phases can fill this cracking, which delays the increase of the pressure in the porous materials and thus the resulting stress. As a result, the restraint stress is not so high as evaluated with the elastic assumption.

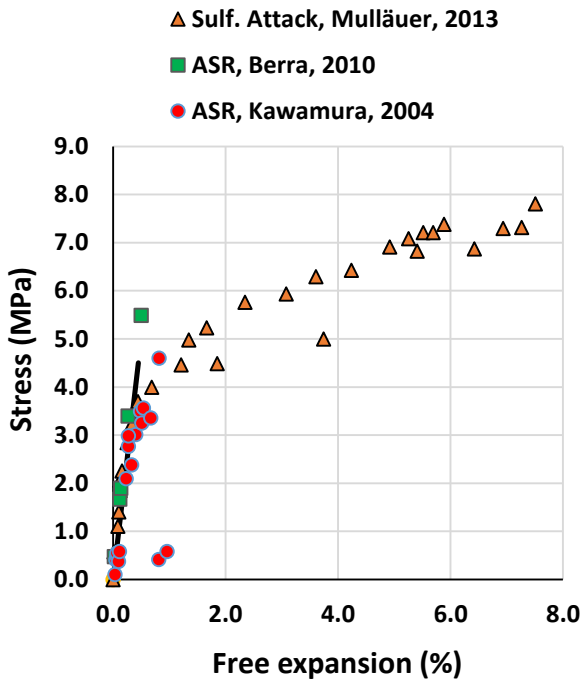

Figure 4: Restraint stress according to expansion in stress free condition for ASR-gels and ettringite in different strong restraint conditions [30], [35], [36].

This behaviour is taken into account through the combination of the pressure equation (Equation (1)) with the following hardening law (17). First, when cracking occurs, the volume of diffuse cracks φ_{cr} increases. The pressure p_i (Equation (1)) and the resulting macroscopic stress cannot increase too much. However, the first crack occurs in the weakest zone of the matrix. The tensile strength of the material after the first cracking increases continuously. The cracking process can continue only if the pressure grows in the zone that is not yet damaged. The stress has to increase in the undamaged zone (as observed in Figure 4) despite the fact that the specimen is free to swell in two directions (and restrained only in one direction). In this aim, a hardening law is proposed. This law has to be anisotropic as explained above:

$$\begin{cases} R_{tI} = f_t + H \cdot \varepsilon_{pl}^{I} \\ R_{tII} = f_t + H \cdot \varepsilon_{pl}^{II} \\ R_{tIII} = f_t + H \cdot \varepsilon_{pl}^{III} \end{cases} \quad (17)$$

with ε_{pl}^{I}, the plastic deformation in the main direction I. It represents the diffuse crack opening in this direction. The sum of the plastic deformations in the three directions is equal to φ_{cr}, the volume of diffuse cracks due to the pressure:

$$\varphi_{cr} = \varepsilon_{pl}^{I} + \varepsilon_{pl}^{II} + \varepsilon_{pl}^{III} \tag{18}$$

and

$$H = h_{crk} \cdot E \tag{19}$$

with h_{crk} the relative slope of the hardening law after cracking and E the elastic modulus of the macro scale material before cracking.

Accurate evaluation of stress level for restraint expansions is obtained by the combination of this hardening law with damage (Equation (11)) and creep modelling. The steeper the slope of the hardening law after cracking, the higher the restraint stress obtained for a given expansion. Figure 4 shows that the hardening law can be approximated by a linear law for expansion lower than about 0.4%. The law should be nonlinear for higher expansion (or at least bi-linear for the domain after cracking to consider the stiffness decrease of the matrix). In this paper, h_{crk} is equal to 0.025 except when this parameter is the object of a parametric study.

For triaxial compressive applied loading, pressures first have to counteract the compressive stress before inducing tension and have to be still greater to cause cracks. For such multiaxial loading, the experiments in the literature show that the measured volumetric expansion decreases [56], [57]. In the model, as long as the cracking criterion (Equation (15)) is not reached, the volume of cracking, φ_{cr}, stays equal to zero and the pressure p_i increases (Equation (1)). As the pressure increases, φ_i^0, the volumetric fraction of new phases leading to small expansion also increases (Equation (2)) to reproduce the dependence on pressure of the migration of phases in connected porosity [56]. Thus, the pressure can never be too high even for triaxial compressive applied loading [61] and the resulting volumetric expansion decreases.

The implementation of this model is based, first, on a classical implicit return mapping algorithm [62] to solve the elasto-plastic problem, then the damage model [42] is applied

to the stresses deduced from the poro-plastic solution. The return mapping algorithm and the damage models are implemented in a non-linear finite element code. The method consists of first computing the evolution of the chemical reaction [63] versus the time step. Then, assuming visco-elastic behaviour of the poro-mechanical media, pressure and stress increments are computed according to the increment of strain. Once these increments have been added to the values of the last time step, the plastic criteria (15) are tested. If the criteria are exceeded, plastic flow is activated to return to the yield functions through the return mapping implicit method and the admissible stress state and pressure state obtained are used in the damage model to assess the apparent stress state. The finite element algorithm then computes the balance between the external forces applied to the structure and the internal forces corresponding to the stresses. If a force balance is not reached, the algorithm corrects the displacement field until equilibrium is reached.

4. Applications

The aim of this part is to evaluate the capability of the model to reproduce expansions in concrete in several situations. The validation is performed on concrete subjected to expansion due to alkali-silica reaction drawn from [50], [54]. In this study, the expansion occurred in reactive silica embedded in non-reactive limestone for two sizes of aggregates (Table 1). Thus, upscaling and calculations based on several pressures were used. The Young's moduli of the new phases, aggregate and concrete were taken to be 7 GPa [64], [65], 60 GPa [43] and 37.3 GPa [50] respectively. The moduli of the different phases used in the calculations are given in Table 2. The concrete tensile and compressive strengths were 4 and 38.4 MPa [50]. The behaviour of concrete in creep is available in [54].

In this application, the advancement was evaluated through mass balance equations solved for each size of aggregates, taking account of alkali diffusion (Equation (20)) and reactive mechanisms deduced from alkali fixation by ASR-gels (Equation (21)) [63]:

$$\begin{cases} p_{agg} S_r \dfrac{\partial [Na^+]}{\partial t} = div\left(D_a \overrightarrow{grad}[Na^+]\right) - \dfrac{\partial Na_f}{\partial t} & (20) \\ \dfrac{\partial Na_f}{\partial t} = \dfrac{\langle [Na^+] - [Na^+]^{thr}_{(Ca,T)} \rangle^+}{\tau_{ASR}} & (21) \end{cases}$$

with p_{agg} the aggregate porosity, S_r the degree of water saturation, $[Na^+]$ the alkali concentration in solution, Na_f, the amount of alkali bound in ASR-gels, D_a, the coefficient of diffusion of alkali in the aggregate, τ_{ASR}, the characteristic time of silica attack and $[Na^+]^{thr}_{(Ca,T)}$ the alkali concentration threshold below which the reaction products cause negligible expansion. This threshold depends on temperature T and calcium concentration, $[Ca^{2+}]$. In first approach, empirical relations can be used:

$$\begin{cases} [Na^+]^{thr}_{(Ca,T)} = 1540 \cdot exp\left[-\frac{205900}{R} \cdot \left(\frac{1}{T} - \frac{1}{T_0}\right)\right] \cdot [Ca^{2+}] & (22) \\ [Ca^{2+}] = 0.357 \cdot exp(386.8 \cdot [Na^+] - 0.01 \cdot T - 1.36 \cdot [Na^+] \cdot T) & (23) \end{cases}$$

With T in Kelvin and T_0, equal to 293 K.

Usually, the molar ratio between silica (SiO_2) and alkali (Na_2O) present in ASR-gels in laboratory conditions is about 5 [64], [66]. The advancement of ASR-gel moles produced by one size of aggregate is then equal to the number of moles of silica attacked by alkalis divided by the maximal number of moles of the new products which can be formed in the aggregate:

$$A_a(t) = \frac{\frac{5}{2}\frac{\partial Na_f}{\partial t}}{n_i^{max}} \quad (24)$$

The fraction of new phases created before cracking, φ^a_{ref}, per volume of aggregate a (Equation (2)) was evaluated from the surface area of the aggregates. In this work, it was taken to be:

$$\varphi^a_{ref} = 1 - \frac{\left(R_a - d_{ref}\right)^3}{R_a^3} \quad (25)$$

with R_a the mean radius of the aggregate a and d_{ref} the distance used to evaluate the volume of new phases created before diffuse cracking. In reality, the volume of new phases formed before cracking is partly included in the aggregate porosity. For the sake of simplicity, only an average distance, d_{ref}, around the aggregate is considered. It is assumed not to depend on the aggregate size. The reference pressure (Equation (2)) is the pressure leading to the first diffuse cracking. p_{ref} depends on the tensile strength of the

porous material, f_t, and on aggregate shape through the stress concentration factor k_I (Figure 2):

$$p_{ref} = \frac{f_t}{k_I} \tag{26}$$

Table 1: Distribution of the aggregate embedded in the concrete studied [50], [54]

Aggregate reference (a)	Aggregate size (mm)	φ_a	b_a
1	4-12	0.10	0.19
2	12-20	0.32	0.49

Table 2: Mechanical properties of the different phases

Properties	New phases	Aggregate	Concrete
Young's modulus (GPa)	7	60	37.3
Poisson's ratio	0.2	0.2	0.2
Bulk modulus K (GPa)	3.9	33.3	20.7
Shear modulus μ (GPa)	2.9	25	15.5

4.1 Anisotropy in stress-free conditions

The model is first used to reproduce the anisotropic expansion due to a natural defect of the materials (Figure 2). In concrete, water pockets can form under aggregate particles, leading to stress concentrations (Figure 2) and thus to anisotropy [43], [53]. For the aggregate used in these experimentations, expansion was anisotropic in stress-free conditions: twice as large in the vertical direction as in the horizontal ones (circles in Figure 5). Isotropic expansion (calculated as the average expansion in the three directions

to obtain the same volumetric expansion – triangles in Figure 5) was first modelled with the following parameters:

- the coefficient of diffusion of alkali in aggregate, D_a: 5.e^{-14} m²/s,
- the characteristic time of silica attack, τ_{ASR}: 400 days,
- the molar volume of new phases, φ_{np}^{mol}: 15.5 cm^3/mol,
- the average distance used to represent the volume of new phases created before diffuse cracking, d_{ref}: 5 µm.

The four parameters have been calibrated on the experimental data to reproduce the isotropic expansions (Figure 5). They can be compared to experimental data of the literature. The coefficient of diffusion of alkali in aggregate is smaller than the coefficients measured in [67]. But such measurements are scarce, and the technique used in this experimental work can be not totally representative of mechanisms occurring during ASR-attack. The characteristic time of attack is slightly larger than the time determined in [68] for opal, which can be expected due to the difference of silica nature (opal is more reactive than aggregate used in this application). Molar volume of synthetic gels similar to natural ASR gels in solution was measured to be between 17 and 24 cm^3/mol depending on the composition of the gels [69]. The calibration is thus in good agreement with these experimental values obtained on synthetic gels. As d_{ref} is an average distance, it cannot be directly compared to microscopic observations. However, it can be supposed to be realistic as it is lower than usual interfacial transition zone between aggregate and cement paste which can reach 20 µm [70], [71].

φ_{np_a}, the volume of new phases of the aggregate *a* at the time step *t* (Equation (7)), is proportional to the molar volume of new phases φ_{np}^{mol} according to the advancement of the reaction (Equation (6)). In this calculation, it leads to final volumes of gel φ_{np_1} and φ_{np_2} respectively equal to 1.9e-2 and 0.9e-2 m^3 of new phases per m^3 of aggregate (Table 3). As the kinetics is partly driven by ionic diffusion in spherical particles, the volume of new phases is the largest in the smallest reactive aggregate. The Biot coefficients and moduli computed for the new phases are given in Table 3. The Biot coefficient of the new phases in the smallest aggregate is larger than that in the largest

aggregate because of differences of volume of the phases. In this experiment, not all the reactive silica was consumed at the end of expansion. If all the silica had been consumed in all the aggregates, the same volume of new phases would have been created per volume of aggregate and thus the Biot coefficients would have been equal for the two aggregates.

The rate of anisotropy, ρ_{ani}, is then calibrated (and taken equal to 0.83) to obtain the anisotropic expansion (Figure 5). The criterion proposed in Equations (15) and (16) used with Equation (14) to obtain anisotropic cracking is then effective to reproduce the anisotropy of expansion in stress-free conditions with the same parameters (φ_{np}^{mol} and d_{ref}) as the averaged isotropic expansion. The formulation of the plasticity law for materials with high anisotropy of expansion in stress-conditions is thus validated. This feature of the model should be also supported by the comparison with expansion of the same material submitted to other stress levels. But experimental data with high anisotropic expansion are scarce and no experimental program have supplied data under various stress state for such materials.

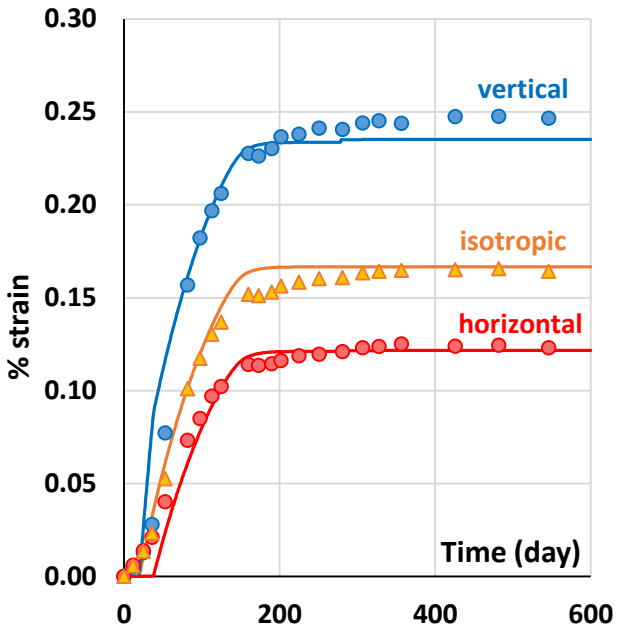

Figure 5: Isotropic or anisotropic stress-free expansion (circles: experimental points [50]*, triangles: averaged isotropic expansion deduced from experimental points, lines: modelling)*

Table 3: Final volume of new phases and Biot coefficient and modulus for each aggregate class

Aggregate size	mm	4-12	12-20
φ_{np_a}	-	1.9e-2	0.9e-2
b_{np}	-	3.8e-2	1.8e-2
M_{np}	GPa	199.	429.

4.2 Expansion under restraint

The dependence of expansion on stress has to be well reproduced in order to obtain relevant modelling of real cases in specimens subjected to gradients or in real structures subjected to external loading or restraint due to boundary conditions. In the macro modelling proposed in [11], [61], which is efficient to reproduce structural behaviour, the Biot modulus and coefficient were used as calibration parameters to reproduce the behaviour of concrete subject to expansion and under mechanical loading and restraint. In the present work, the Biot modulus and coefficient are determined from the volume of new phases and from the mechanical properties of concrete, aggregate and new phases. In this case, only the slope of the hardening law after cracking h_{crk} in equation (18) is unknown. This parameter allows the pressure growth to be determined during the cracking process needed to explain the longitudinal stress increase observed in the experiments reported in Figure 4. The present paper proposes a parametric study to verify the capability of the model to reproduce the dependence of expansion on stress with only the slope of the hardening law as calibration parameter.

The impact of h_{crk} on restrained stress is studied first. Three sets of parameters (Table 4) are determined for three significantly different values to obtain the same stress-free expansion (about 0.17% of isotropic linear expansion in Figure 5). The greater the slope of the hardening law, h_{crk}, the greater the pressure increase and the axial stress after cracking. In consequence, the molar volume φ_{np}^{mol} necessary to obtain the same stress-free expansion has be to larger for a greater h_{crk}. This is due to the fact that, when

pressure growth is possible (when h_{crk} is great enough), the amount of gel migrating to the connected porosity also increases (see Equation (2)), so the amount of gel remaining in the inclusion to maintain the pressure would be smaller if the molar volume was not increased artificially to retrieve the correct free swelling.

Table 4: Modelling parameters for the study of restraint stress

h_{crk}	φ_{np}^{mol}	d_{ref}
-	(cm^3/mol)	(µm)
0.002	14.	4.5
0.025	15.5	5.
0.2	27.5	6.

Expansion under uniaxial restraint is then modelled. In this aim, the strain has been set to zero in the restraint direction. The numerical restraint stresses are plotted in Figure 6 for the three values of slope: the greater the slope, the larger the restraint stress. For h_{crk} equal to 0.002, the restraint stress is close to zero. This means that the pressure remains almost constant during crack propagation, as can happen for very fluid new phases (Figure 4 and Figure 7). In most cases, the restraint stress is about 1 MPa for 0.1% expansion and up to 0.4 or 0.5% expansion (Figure 7). A correct mean representation is obtained for a slope of about 0.025 (restraint stress of about 1.65 MPa for a final isotropic expansion of about 0.17%, Figure 7). For h_{crk} equal to 0.2, the calculation is closer to the elastic calculation than in the previous cases and restraint stress becomes too high (Figure 6 and Figure 7). The end of the production of new phases occurs at about 180 days and free expansion stabilizes by this date (Figure 5). For restraint expansion, after the stabilization of expansion, a decrease of the restraint stress can be observed (Figure 6). It is due to the concrete relaxation, which is caused by the concrete viscoelastic behaviour, here, fitted on creep tests [41].

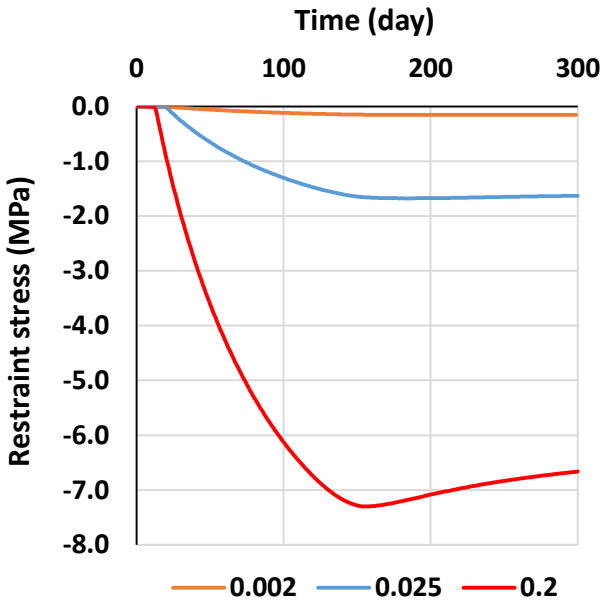

Figure 6: Restraint stress for an expansion of about 0.16% according to h_{crk}

510

511 In this paper, the calibration of the parameter h_{crk} has been performed to obtain a
512 restraint stress of about 1 MPa for an expansion in stress-free conditions of about 0.1%
513 (h_{crk} equal to 0.025). It is a usual mean value for expansive mechanisms under restraint.
514 The modelling validation is performed in Figure 7 with the comparison with several
515 experimental studies *[30]*, *[35]*, *[36]*. These works were performed for different initial
516 materials and different new phases (ASR or ettringite). The modelling is able to evaluate
517 the stress for restrained expansion of the three experimental studies, if expansion in
518 stress-free condition is lower than 0.4%. A non-linear hardening law could give better
519 results for larger expansions but the calculations would be more time-consuming (in
520 cases of linear hardening, the implicit return mapping algorithm converges in one step
521 only, which is no longer the case for nonlinear hardening). For phenomena with greater
522 expansion (delayed ettringite formation, sulfate attack), a multi-linear description could
523 lead to a more realistic evaluation without consuming too much computational time.

524 In some experiments, very small stress was noted for material with large potential for
525 expansion in stress free conditions (Figure 7, [35]). It was due to exudation of products
526 out of the specimens as observed by the authors of [35]. Such phenomena are not intrinsic

to the material and should not be reproduced by material modelling but by coupled modelling as proposed in [72]. Future works will combine the present modelling with transport modelling to reproduce such mechanisms.

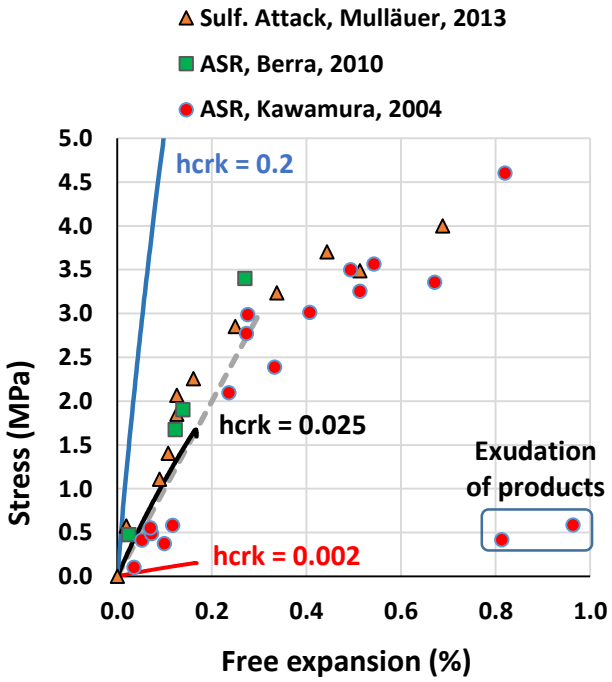

Figure 7: Restraint stress according to expansion in stress free condition, comparison with modelling according to h_{crk} (from 0.002 to 0.2), experimental data from [30], [35], [36]

4.3 Irreversibility of expansion during drying

The aim of this part is to analyse the ability of the model to reproduce the behaviour of concrete undergoing first expansion then drying shrinkage. After 650 days of expansion for the concrete analysed in part 3.1, specimens were exposed to air at 30% RH [50]. When the new phases due to alkali-silica reaction dried, their volume decreased because of water loss, but the concrete expansion did not change; only the usual concrete drying shrinkage occurred (Figure 8, [50]).

For the calculations below, the same parameters as in part 3.1 are used for expansion. Drying shrinkage is obtained through the Van Genuchten model [73] as explained in [41]. In this case, Equation (9) becomes:

$$\tilde{\sigma_s} = K_d \cdot \left(\varepsilon - \varepsilon_{an}\right) - \sum_a b_a \cdot p_a - b_w \cdot p_w \quad (27)$$

with b_w, the Biot coefficient of water (dependent on the saturation degree of the porosity in the material). p_w is the pressure due to water, which is negative in case of shrinkage (due the capillarity effect) and zero during swelling in water. The pressure p_w is modelled using the Van Genuchten model [73]:

$$p_w = -M_{shr} \cdot \left(S_r^{-\frac{1}{m_{vg}}} - 1\right)^{(1-m_{vg})} \quad (28)$$

M_{shr} and m_{vg} can be calibrated on the water retention curve or on the evolution of shrinkage strains.

In the present work, the Biot coefficient of water b_w has been evaluated from the concrete porosity (16%) [74]. It is equal to 0.4 for this concrete in case of total saturation. m_{vg} has been taken equal to the usual value 0.5, and only M_{shr} has to be calibrated. M_{shr} is evaluated to reproduce the shrinkage strain on a concrete which has never been damaged by ASR (Figure 8-a). It is equal to 32 MPa, which is a usual value for concrete [41]. The validation of the model is performed on the same concrete which is submitted to the same drying but after ASR expansion (Figure 8-b). After expansion occurring in water, concrete shrinks with the usual dependence on water pressure (Figure 8-b). Cracking induced by the formation of the new phases did not change the amplitude of shrinkage significantly since the experimental results could be found without changing the coefficients of Equations (27) and (28) after swelling. The decrease of ASR-gel volumes induced by the drying did not impact the irreversible expansion: they were either filled by crystallized phases or were impossible to reclose simply because of the roughness of their lips. Figure 8-b shows that the behaviour observed on specimens can be reproduced by a basic combination of poromechanics (Equation (27)) with the linear anisotropic plasticity used in the constitutive equations.

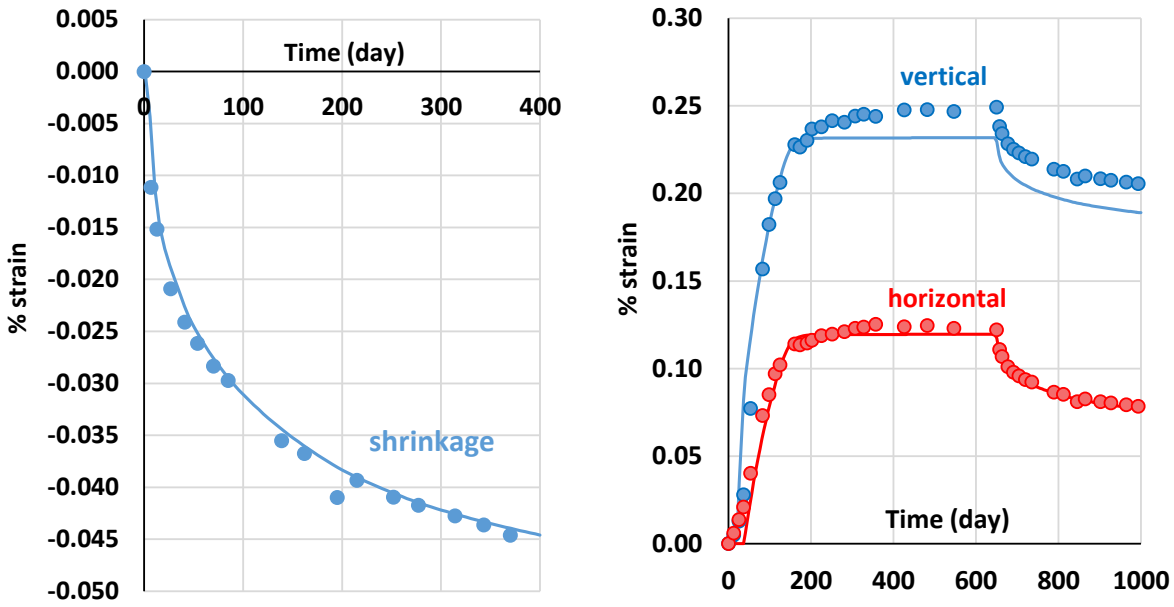

(a) *(b)*

Figure 8: Calibration of shrinkage parameters on concrete which has never been damaged by ASR (a) and validation on the same concrete which is submitted to the same drying, after ASR expansion (b) (circles: experimental points [50]*, lines: modelling)*

4.4 Damage due to pressure gradient

In the previous analysis, homogeneous conditions were assumed so as to analyse the response of the model from a material point of view without disturbance due to gradient effects. In reality, the specimens analysed just above were kept in water. Such storage leads to a pressure gradient due to alkali leaching: close to the specimen skin, alkalis leach out rapidly and cannot participate in the chemical reaction. As a result, chemical advancement is slower close to the skin than in specimen cores, which leads to pressure gradients and skin cracking. In the calculations, the risk of skin cracking and the cracks opening is evaluated by the model presented in [42]. The model is regularized with Hillerborg anisotropic method to avoid mesh dependence [75]. The calibration of the expansion curves in the two directions (Figure 9) is obtained for a molar volume of new phases, φ_{np}^{mol}, equal to 22.1 cm^3/mol, an average distance over which the new phases can

575 move without causing cracking, d_{ref}, equal to 7 µm, and the anisotropy ratio, ρ_{ani}, equal
576 to 0.82. The radial deformation is the radial displacement in P1 divided by the specimen
577 radius, and the vertical deformation is the vertical displacement in P2 divided by the
578 measurement basis (five centimetres above the symmetry axis as during experimentation
579 – Figure 10). As a fraction of the reactants does not participate in the attack because of
580 their leaching, the molar volume has to be slightly higher than in the previous
581 calculations to obtain the same expansion. The gradient of advancement due to alkali
582 leaching leads to the pressure gradient presented in Figure 10-a. Thus, tensile stresses at
583 the external surface of concrete specimens (Figure 10-b) are sufficient to cause localized
584 cracking with openings larger than 100 µm (Figure 11), which is the cracking often
585 observed on specimens in laboratory and real structures. Such a gradient can be induced
586 by leaching or drying according to the environmental conditions (open cracks visible
587 without microscopic tools, Figure 12) [1]. The diffuse cracking due to pressure is usually
588 finer and forms a denser network (one or two cracks per aggregate [48]) and can also be
589 observed on real structures sometimes (Figure 12).
590

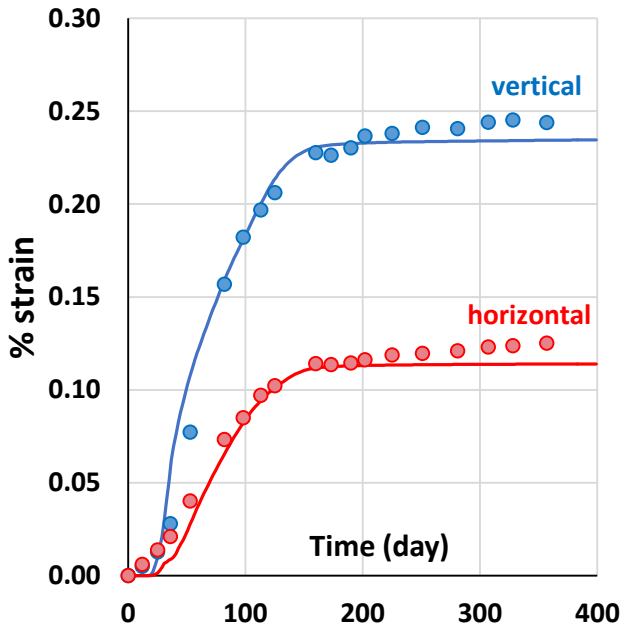

Figure 9: Comparison of calculated expansion and experimental data (circles: experimental points [50])

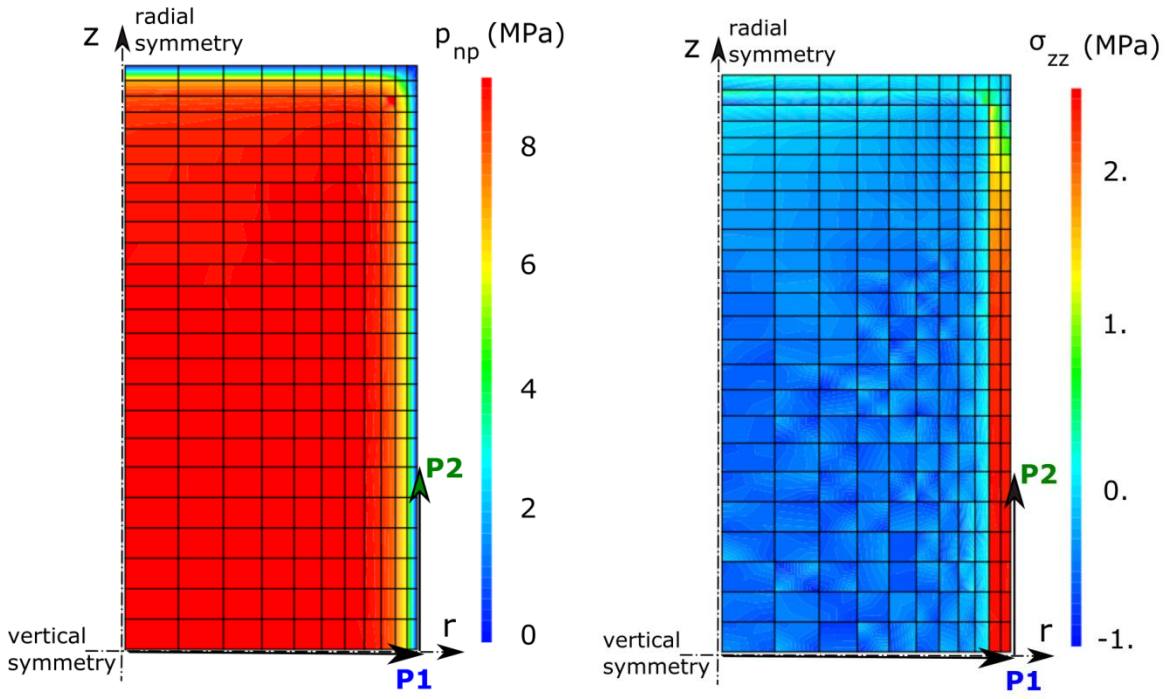

(a) (b)

Figure 10: Pressure gradient due to alkali leaching (a) and induced stresses (b) just before skin cracking (in MPa)

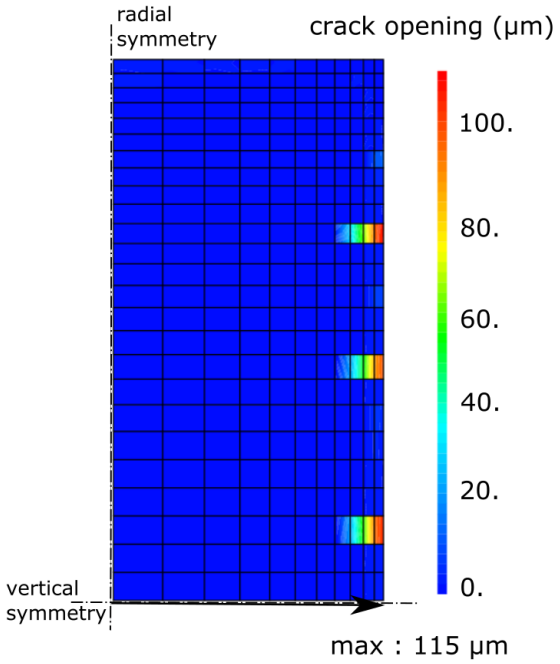

Figure 11: Cracking due to pressure gradient at the end of the test

591

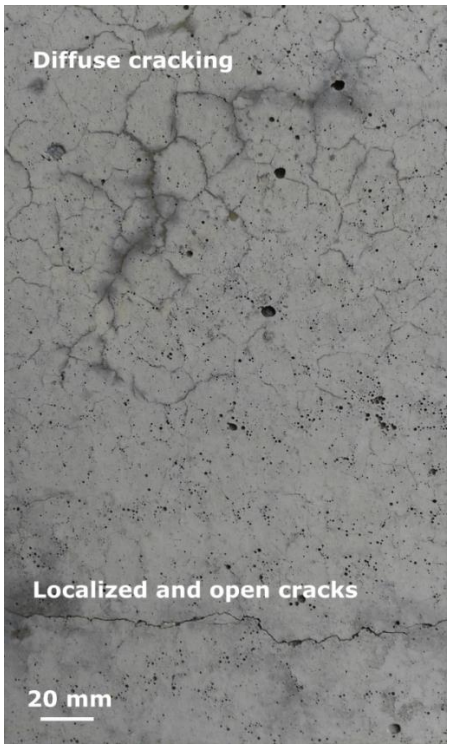

Figure 12: Diffuse and localized cracks on column damaged by expansive phenomena

592

593 Investigations showed that expansive materials were usually subjected to a pressure
594 gradient due to environmental conditions, even in laboratory tests performed on small
595 specimens. Gradients of temperature, moisture or ionic species lead to gradients of
596 pressure. Such gradients can lead to localized open cracks on the skin or in the core of
597 specimens. This strongly impacts the expansion measurements and the consequences in
598 terms of material damage evaluated on specimens. Diffuse and localized cracking do not
599 have the same impact in terms of strength and rigidity decreases and of transfer
600 properties. In the future, models will have to assess the crack opening due to pressure
601 gradients in real structures as it will impact the durability of the structure through the
602 induced modifications of transfer properties. Such an assessment can be performed from
603 crack openings for localized cracks or for diffuse cracking. Therefore, modelling of
604 expansive phenomena should be able to distinguish between diffuse damage due to
605 pressure and localized damage due to gradient. In this work, the distinction is achieved by
606 combining the plasticity modelling, used to represent the permanent strain due to diffuse

607 cracking induced by pressure presented above, with the damage modelling presented in
608 [42].

609 ## *4.5. Discussion*

610 The previous calculations were performed in the framework of poromechanics. The Biot
611 coefficient and modulus depend on the mechanical properties of the materials and on the
612 volume of porosity filled by the new phases. For the multi-scale modelling used to assess
613 the impact of alkali-silica reaction, the Biot coefficients of new phases in aggregate,
614 evaluated through Equation (5), lie between 3.8e-2 (in homogeneous conditions) and
615 5.4e-2 (in the calculations with gradient) in the smallest aggregate (4/12) and between
616 1.8e-2 and 2.5e-2 in the largest one (12/20) at the end of the calculated expansion. These
617 values are consistent with previous calculations performed for other new phases formed
618 in concrete [12], [13]. The Biot coefficients of aggregate in concrete reach about 0.2 in
619 the smaller aggregate (4/12) and 0.5 in the larger aggregates (4/12). This is consistent
620 with modelling that evaluates the expansion from the action of the aggregate on the
621 concrete [26], [61], [76] without representation of aggregate damage. It is usually
622 performed in structural calculations. The modelling proposed in this paper makes the link
623 between the two scales. Taking the shape of cracks into consideration could lead to
624 slightly larger coefficients [26], [40]. This means that the present modelling could
625 underestimate the percentage of expansion due to pressure and thus slightly overestimate
626 the percentage due to cracking. Pressure due to the formation of new phases and
627 evaluated by the present modelling lies between 10 and 15 MPa. These values are
628 consistent with usual values measured for such new phases [77], [78] or evaluated
629 through theoretical approaches [79], [80]. It is also a validation of the mechanical
630 developments proposed in this paper.
631

5. Conclusion

The main consequences of expansion in quasi-brittle materials are: anisotropic induced cracking due to natural causes or due to external loading, stress for restrained expansion, irreversibility of diffuse cracking and localized cracks due to pressure gradients.

A model of expansion in quasi-brittle materials has been proposed. It is based on poromechanics and on a plastic, anisotropic criterion to represent permanent strain due to diffuse cracking caused by pressure. Thus the anisotropy of cracking is induced by the addition of local stress due to pressure and external loading. Equations have been proposed for multiple pressures to take account of the effects of differences of advancement in the formation of new products on pressure and induced damage.

The following physical phenomena can be reproduced by the model:

- Anisotropy of expansion and cracking due to the initial anisotropy properties of the material,
- Induced stress in conditions of restraint,
- Irreversibility of expansion during drying periods,
- Shrinkage of cracked drying concrete previously affected by expansion,
- Combination of diffuse damage due to expansion and localized damage due to gradient.

The importance of diffuse cracking in the mechanisms of expansion in concrete has been highlighted. This mechanical behaviour is strongly dependent on the mechanical properties of the material subjected to expansion and particularly to properties in tension: first for the diffuse damage and the direction of cracking due to pressure and, second, for the localized cracks due to pressure gradient. The latter point introduces the quantification of localized crack opening to evaluate the consequences of damage due to a skin gradient in terms of mechanical and transfer properties. Cracks are usually observed along reinforcements in structures subjected to expansion. These cracks shorten the service life of damaged structures and the reduction can be evaluated from the crack opening. This is an important issue when modelling the durability of structures affected by expansion.

661

662 6. References

663 [1] B. Fournier and M.-A. Bérubé, “Alkali-aggregate reaction in concrete : A review
664 of basic concepts and engineering implications,” *Can. J. Civ. Eng.*, vol. 27, pp.
665 167–191, 2000.

666 [2] S. Diamond, “Delayed ettringite formation - Processes and problems,” *Cem.*
667 *Concr. Compos.*, vol. 18, pp. 205–215, 1996.

668 [3] C. Ouyang, A. Nanni, and W. F. Chang, “Internal and external sources of sulfate
669 ions in Portland cement mortar; two types of chemical attack,” *Cem. Concr. Res.*,
670 vol. 18, pp. 699–709, 1988.

671 [4] M. Neji, B. Bary, P. Le Bescop, and N. Burlion, “Swelling behavior of ion
672 exchange resins incorporated in tri-calcium silicate cement matrix: I. Chemical
673 analysis,” *J. Nucl. Mater.*, vol. 467, pp. 544–556, 2015.

674 [5] C. Huang and R. Feldman, “Dependence of Frost Resistance on the Pore Structure
675 of Mortar Containing Silica Fume,” *ACI J.*, vol. 82, no. 5, pp. 740–743, 1985.

676 [6] O. Coussy, *Poromechanics*, Wiley. New York, 2004.

677 [7] L. Dormieux, D. Kondo, and F. Ulm, *Microporomechanics*, Wiley. 2006.

678 [8] J. Lubliner, J. Oliver, S. Oller, and E. Onate, “A plastic-damage model for
679 concrete,” *Int. J. Solids Struct.*, vol. 25, no. 3, pp. 299–326, 1989.

680 [9] A. D. Jefferson, “Craft — a plastic-damage-contact model for concrete . I . Model
681 theory and thermodynamic considerations,” *Int. J. Solids Struct.*, vol. 40, pp.
682 5973–5999, 2003.

683 [10] B. Capra and A. Sellier, “Orthotropic modelling of alkali-aggregate reaction in
684 concrete structures : numerical simulations,” *Mech. Mater.*, vol. 6, no. December,
685 2002.

686 [11] E. Grimal, A. Sellier, Y. Le Pape, and E. Bourdarot, “Creep, Shrinkage, and
687 Anisotropic Damage in Alkali-Aggregate Reaction Swelling Mechanism-Part I. A
688 Constitutive Model,” *ACI Mater. J.*, vol. 105, no. 3, pp. 227–235, 2008.

689 [12] B. Bary, N. Leterrier, E. Deville, and P. Le Bescop, “Coupled chemo-transport-
690 mechanical modelling and numerical simulation of external sulfate attack in
691 mortar,” *Cem. Concr. Compos.*, vol. 49, pp. 70–83, 2014.

692 [13] B. Bary, “Simplified coupled chemo-mechanical modeling of cement pastes
693 behavior subjected to combined leaching and external sulfate attack,” *Int. J.*
694 *Numer. Anal. Methods Geomech.*, vol. 32, no. February, pp. 1791–1816, 2008.

695 [14] R. J. Flatt and G. W. Scherer, “Thermodynamics of crystallization stresses in
696 DEF,” *Cem. Concr. Res.*, vol. 38, pp. 325–336, 2008.

697 [15] R. Tixier and B. Mobasher, “Modeling of Damage in Cement-Based Materials
698 Subjected to External Sulfate Attack . I : Formulation,” *ASCE J. Mater. Civ. Eng.*,

vol. 15, no. August, pp. 305–313, 2003.

[16] A. E. Idiart, C. M. López, and I. Carol, “Chemo-mechanical analysis of concrete cracking and degradation due to external sulfate attack : A meso-scale model,” *Cem. Concr. Compos.*, vol. 33, pp. 411–423, 2011.

[17] S. Sarkar, S. Mahadevan, J. C. L. Meeussen, H. Van Der Sloot, and D. S. Kosson, “Numerical simulation of cementitious materials degradation under external sulfate attack,” *Cem. Concr. Compos.*, vol. 32, no. 3, pp. 241–252, 2010.

[18] N. Cefis and C. Comi, “Chemo-mechanical modelling of the external sulfate attack in concrete,” *Cem. Concr. Res.*, vol. 93, pp. 57–70, 2017.

[19] A. Gholizadeh, F. Rajabipour, and J. L. Rosenberger, “Composition – rheology relationships in alkali – silica reaction gels and the impact on the gel’s deleterious behavior,” *Cem. Concr. Res.*, vol. 83, pp. 45–56, 2016.

[20] W. Puatatsananon and V. Saouma, “Chemo-mechanical micromodel for alkali-silica reaction,” *ACI Mater. J.*, vol. 110, no. 110, pp. 67–77, 2013.

[21] M. Alnaggar, G. Cusatis, and G. Di Luzio, “Lattice Discrete Particle Modeling (LDPM) of Alkali Silica Reaction (ASR) deterioration of concrete structures,” *Cem. Concr. Compos.*, vol. 41, pp. 45–59, 2013.

[22] G. W. Scherer, “Crystallization in pores,” *Cem. Concr. Res.*, vol. 29, no. December 1998, pp. 1347–1358, 1999.

[23] O. Coussy, “Deformation and stress from in-pore drying-induced crystallization of salt,” *J. Mech. Phys. Solids*, vol. 54, pp. 1517–1547, 2006.

[24] O. Coussy, “Poromechanics of freezing materials,” *J. Mech. Phys. Solids*, vol. 53, pp. 1689–1718, 2005.

[25] Q. Zeng, T. Fen-Chong, P. Dangla, and K. Li, “A study of freezing behavior of cementitious materials by poromechanical approach,” *Int. J. Solids Struct.*, vol. 48, no. 22–23, pp. 3267–3273, 2011.

[26] L. Charpin and A. Ehrlacher, “Microporomechanics study of anisotropy of ASR under loading,” *Cem. Concr. Res.*, vol. 63, pp. 143–157, 2014.

[27] A. Sellier, J. P. Bournazel, and A. Mébarki, “Une modélisation de la réaction alcalis-granulat intégrant une description des phénomènes aléatoires locaux,” *Mater. Struct.*, vol. 28, no. 1, pp. 373–383, 1995.

[28] L. Charpin and A. Ehrlacher, “Simplified model for the transport of Alkali-Silica Reaction gel in concrete porosity,” *J. Adv. Concr. Technol.*, vol. 12, pp. 1–6, 2014.

[29] Z. Bažant and S. Rahimi-Aghdam, “Diffusion-Controlled and Creep-Mitigated ASR Damage via Microplane Model . I : Mass Concrete,” *J. Eng. Mech.*, vol. 143, no. 3, pp. 1–10, 2017.

[30] W. Müllauer, R. E. Beddoe, and D. Heinz, “Sulfate attack expansion mechanisms,” *Cem. Concr. Res.*, vol. 52, pp. 208–215, 2013.

[31] T. Ichikawa, “Alkali-silica reaction, pessimum effects and pozzolanic effect,” *Cem. Concr. Res.*, vol. 39, pp. 716–726, 2009.

739 [32] T. Ichikawa and M. Miura, “Modified model of alkali-silica reaction,” *Cem.*
740 *Concr. Res.*, vol. 37, pp. 1291–1297, 2007.

741 [33] E. Garcia-Diaz, J. Riche, D. Bulteel, and C. Vernet, “Mechanism of damage for
742 the alkali-silica reaction,” *Cem. Concr. Res.*, vol. 36, pp. 395–400, 2006.

743 [34] E. Garcia-Diaz, D. Bulteel, Y. Monnin, P. Degrugilliers, and P. Fasseu, “ASR
744 pessimum behaviour of siliceous limestone aggregates,” *Cem. Concr. Res.*, vol. 40,
745 no. 4, pp. 546–549, 2010.

746 [35] M. Kawamura and K. Iwahori, “ASR gel composition and expansive pressure in
747 mortars under restraint,” *Cem. Concr. Compos.*, vol. 26, pp. 47–56, 2004.

748 [36] M. Berra, G. Faggiani, T. Mangialardi, and a. E. Paolini, “Influence of stress
749 restraint on the expansive behaviour of concrete affected by alkali-silica reaction,”
750 *Cem. Concr. Res.*, vol. 40, pp. 1403–1409, 2010.

751 [37] H. Kagimoto, Y. Yasuda, and M. Kawamura, “ASR expansion, expansive pressure
752 and cracking in concrete prisms under various degrees of restraint,” *Cem. Concr.*
753 *Res.*, vol. 59, pp. 1–15, 2014.

754 [38] H. Bouzabata, S. Multon, A. Sellier, and H. Houari, “Effects of restraint on
755 expansion due to delayed ettringite formation,” *Cem. Concr. Res.*, vol. 42, no. 7,
756 pp. 1024–1031, 2012.

757 [39] K. Mori and K. Tanaka, “Average stress in matrix and average elastic energy of
758 materials with misfitting inclusions,” *Acta Mettalurg.*, vol. 21, no. 5, pp. 1605–
759 1609, 1973.

760 [40] R. Esposito and M. A. N. Hendriks, “A multiscale micromechanical approach to
761 model the deteriorating impact of alkali-silica reaction on concrete,” *Cem. Concr.*
762 *Compos.*, vol. 70, pp. 139–152, 2016.

763 [41] A. Sellier, S. Multon, L. Buffo-Lacarrière, T. Vidal, X. Bourbon, and G. Camps,
764 “Concrete creep modelling for structural applications: non-linearity, multi-axiality,
765 hydration, temperature and drying effects,” *Cem. Concr. Res.*, vol. 79, pp. 301–
766 315, 2016.

767 [42] A. Sellier, G. Casaux-Ginestet, L. Buffo-Lacarrière, and X. Bourbon, “Orthotropic
768 Damage Coupled with Localised Crack Reclosure Processing. Part I: Constitutive
769 Laws,” *Eng. Fract. Mech.*, vol. 97l, no. January, pp. 148–167, Oct. 2013.

770 [43] C. Larive, “Apports combinés de l’expérimentation et de la modélisation à la
771 compréhension de l’alcali-réaction et de ses effets mécaniques, Laboratoire Central
772 des Ponts et Chaussées (Edt.), Ouvrage d’Art, Rapport OA 28,” 1998.

773 [44] F.-J. Ulm, O. Coussy, K. Li, and C. Larive, “Thermo-Chemo-Mechanics of ASR
774 expansion in concrete structures,” *ASCE J. Eng. Mech.*, vol. 126, no. March, pp.
775 233–242, 2000.

776 [45] J. Berard, R. Roux, I. Depuis, and C. Climinces, “La viabilite des betons du
777 Quebec: le role des granulats,” *Can J Civ Eng*, vol. 13, no. 1, pp. 12–24, 1986.

778 [46] J. M. Ponce and O. R. Batic, “Different manifestations of the alkali-silica reaction

779 in concrete according to the reaction kinetics of the reactive aggregate," *Cem.*
780 *Concr. Res.*, vol. 36, pp. 1148–1156, 2006.

781 [47] M. Ben Haha, E. Gallucci, A. Guidoum, and K. L. Scrivener, "Relation of
782 expansion due to alkali silica reaction to the degree of reaction measured by SEM
783 image analysis," *Cem. Concr. Res.*, vol. 37, pp. 1206–1214, 2007.

784 [48] L. F. M. Sanchez, B. Fournier, M. Jolin, and J. Duchesne, "Reliable quantification
785 of AAR damage through assessment of the Damage Rating Index (DRI)," *Cem.*
786 *Concr. Res.*, vol. 67, pp. 74–92, 2015.

787 [49] A. B. Giorla, K. L. Scrivener, and C. F. Dunant, "Influence of visco-elasticity on
788 the stress development induced by alkali–silica reaction," *Cem. Concr. Res.*, vol.
789 70, pp. 1–8, 2015.

790 [50] S. Multon and F. Toutlemonde, "Effect of moisture conditions and transferts on
791 alkali silica reaction damaged structures," *Cem. Concr. Res.*, vol. 40, pp. 924–934,
792 2010.

793 [51] N. Smaoui, M.-A. Bérubé, B. Fournier, and B. Bissonnette, "Influence of
794 Specimen Geometry, Orientation of Casting Plane, and Mode of Concrete
795 Consolidation on Expansion Due to ASR," *Cem. Concr. Aggregates*, vol. 26, no. 2,
796 pp. 1–13, 2004.

797 [52] G. Wardeh and B. Perrin, "Freezing-thawing phenomena in fired clay materials
798 and consequences on their durability," *Constr. Build. Mater.*, vol. 22, pp. 820–828,
799 2008.

800 [53] C. Larive, M. Joly, and O. Coussy, "Heterogeneity and anisotropy in ASR-affected
801 concrete –Consequences for structural assessment," in *11th International*
802 *Conference on Alkali-Aggregate Reaction in Concrete*, 2000, pp. 969–978.

803 [54] S. Multon and F. Toutlemonde, "Effect of applied stresses on alkali-silica reaction-
804 induced expansions," *Cem. Concr. Res.*, vol. 36, no. 5, pp. 912–920, 2006.

805 [55] C. F. Dunant and K. L. Scrivener, "Effects of uniaxial stress on alkali-silica
806 reaction induced expansion of concrete," *Cem. Concr. Res.*, vol. 42, no. 3, pp.
807 567–576, 2012.

808 [56] B. P. Gautam, D. K. Panesar, S. A. Sheikh, and F. J. Vecchio, "Multiaxial
809 Expansion-Stress Relationship for Alkali Silica Reaction-Affected Concrete," *ACI*
810 *Mater. J.*, vol. 114, no. 1, pp. 171–184, 2017.

811 [57] J. Liaudat, I. Carol, C. M. López, and V. E. Saouma, "ASR expansions in concrete
812 under triaxial confinement," *Cem. Concr. Compos.*, vol. doi: 10.10, 2017.

813 [58] H. Kagimoto and M. Kawamura, "Measurements of strain and humidity within
814 massive concrete cylinders related to the formation of ASR surface cracks," *Cem.*
815 *Concr. Res.*, vol. 41, pp. 808–816, 2011.

816 [59] R.-P. Martin, "Analyse sur structures modèles des effets mécaniques de la réaction
817 sulfatique interne du béton, Ph.D. thesis, LCPC Laboratoire Central des Ponts et
818 Chaussées Paris," 2010.

[60] M. Salgues, “Modélisations des effets structuraux des réactions sulfatiques internes et alcali-granulats : Application aux barrages en béton, PhD Thesis, Université de Toulouse,” 2013.

[61] P. Morenon, S. Multon, A. Sellier, E. Grimal, F. Hamon, and E. Bourdarot, “Impact of stresses and restraints on ASR expansion,” *Constr. Build. Mater.*, vol. 140, pp. 58–74, 2017.

[62] J. Simo, *Numerical analysis and simulation of plasticity*. Ciarlet, P., Lions, J. (Eds.), Handbook of Numerical Analysis, vol. VI. North- Holland, 1998.

[63] S. Multon and A. Sellier, “Multi-scale analysis of alkali-silica reaction (ASR): Impact of alkali leaching on scale effects affecting expansion tests,” *Cem. Concr. Res.*, vol. 81, pp. 122–133, 2016.

[64] A. Leemann and P. Lura, “E-modulus of the alkali-silica-reaction product determined by micro-indentation,” *Constr. Build. Mater.*, vol. 44, pp. 221–227, 2013.

[65] C. Zhang, L. Sorelli, B. Fournier, J. Duchesne, J. Bastien, and Z. Chen, “Stress-relaxation of crystalline alkali-silica reaction products : Characterization by micro- and nanoindentation and simplified modeling,” *Constr. Build. Mater.*, vol. 148, pp. 455–464, 2017.

[66] M. Kawamura and H. Fuwa, “Effects of lithium salts on ASR gel composition and expansion of mortars,” *Cem. Concr. Res.*, vol. 33, pp. 913–919, 2003.

[67] S. Goto and D. M. Roy, “Diffusion of ions through hardened cement pastes,” *Cem. Concr. Res.*, vol. 11, pp. 751–757, 1981.

[68] T. Kim, J. Olek, and H. Jeong, “Alkali–silica reaction: Kinetics of chemistry of pore solution and calcium hydroxide content in cementitious system,” *Cem. Concr. Res.*, vol. 71, pp. 36–45, 2015.

[69] A. Perruchot, P. Massard, and J. Lombardi, “Composition et volume molaire apparent des gels Ca–Si, une approche expérimentale,” *C. R. Geosci.*, vol. 335, pp. 951–958, 2003.

[70] K. L. Scrivener and K. M. Nemati, “The percolation of pore space in the cement paste/aggregate interfacial zone of concrete,” *Cem. Concr. Res.*, vol. 26, no. 1, pp. 35–40, 1996.

[71] K. L. Scrivener, A. K. Crumbie, and P. Laugesen, “The interfacial transition zone (ITZ) between cement paste and aggregate in concrete,” *Interface Sci.*, vol. 12, no. 4, pp. 411–421, 2004.

[72] Y. Takahashi, S. Ogawa, Y. Tanaka, and K. Maekawa, “Scale-Dependent ASR Expansion of Concrete and Its Prediction coupled with Silica Gel Generation and Migration,” *J. Adv. Concr. Technol.*, vol. 14, pp. 444–463, 2016.

[73] T. M. Van Genuchten and D. Nielsen, “On describing and predicting the hydraulic properties of unsaturated soils,” *Ann. Phys.*, vol. 3, no. 5, pp. 615–628, 1985.

[74] B. Zuber and J. Marchand, “Modeling the deterioration of hydrated cement

systems exposed to frost action - Part 1: Description of the mathematical model," *Cem. Concr. Res.*, vol. 30, no. 2000, pp. 1929–1939, 2000.

[75] A. Hillerborg, M. Modéer, and P.-E. Petersson, "Analysis of crack formation and crack growth in concrete by means of fracture mechanics and finite elements," *Cem. Concr. Res.*, vol. 6, pp. 773–782, 1976.

[76] C. Comi, B. Kirchmayr, and R. Pignatelli, "Two-phase damage modeling of concrete affected by alkali – silica reaction under variable temperature and humidity conditions," *Int. J. Solids Struct.*, vol. 49, no. 23–24, pp. 3367–3380, 2012.

[77] L. J. Stuble and S. Diamond, "Swelling Properties of Synthetic Alkali Silica Gels," *J. Am. Ceram. Soc.*, vol. 64, no. 11, pp. 652–655, 1981.

[78] H. W. Reinhardt and O. Mielich, "A fracture mechanics approach to the crack formation in alkali-sensitive grains," *Cem. Concr. Res.*, vol. 41, no. 3, pp. 255–262, 2011.

[79] M. Prezzi, P. J. M. Monteiro, and G. Sposito, "The alkali-silica reaction, part I: Use of the double-layer theory to explain the behavior of reaction-product gels," *ACI Mater. J.*, vol. 94, no. 94, pp. 10–17, 1997.

[80] R. Pignatelli, C. Comi, and P. J. M. Monteiro, "A coupled mechanical and chemical damage model for concrete affected by alkali-silica reaction," *Cem. Concr. Res.*, vol. 53, pp. 196–210, 2013.